

Stability analysis of flame fronts: Dynamical systems approach in the complex plane

Oleg Kupervasser, Zeev Olami, and Itamar Procaccia

Department of Chemical Physics, The Weizmann Institute of Science, Rehovot 76100, Israel

(Received 20 August 1998)

We consider flame front propagation in channel geometries. The steady-state solution in this problem is space dependent and therefore the linear stability analysis is described by a partial integro-differential equation with a space-dependent coefficient. Accordingly, it involves complicated eigenfunctions. We show that the analysis can be performed using a finite-order dynamical system in terms of the dynamics of singularities in the complex plane, yielding a detailed understanding of the physics of the eigenfunctions and eigenvalues. [S1063-651X(99)01902-9]

PACS number(s): 05.40.Ca, 47.27.-i

I. INTRODUCTION

In this paper we discuss the stability of steady flame fronts in channel geometry. Traditionally [1–3] one studies stability by considering the linear operator that is obtained by linearizing the equations of motion around the steady solution. The eigenfunctions obtained are *delocalized* and in certain cases are not easy to interpret. In the case of flame fronts the steady-state solution is space dependent and therefore the eigenfunctions are very different from simple Fourier modes. We show in this paper that a good understanding of the nature of the eigenspectrum and eigenmodes can be obtained by doing almost the opposite of traditional stability analysis, i.e., studying the *localized* dynamics of singularities in the complex plane. By reducing the stability analysis to a study of a finite-dimensional dynamical system one can gain considerable intuitive understanding of the nature of the stability problem.

The analysis is based on the understanding that for a given channel width L the steady-state solution for the flame front is given in terms of $N(L)$ poles that are organized on a line parallel to the imaginary axis [4]. The stability of this solution can then be considered in two steps. In the first step we examine the response of this set of $N(L)$ poles to perturbations in their positions. This procedure yields an important part of the stability spectrum. In the second step we examine general perturbations, which can also be described by the addition of extra poles to the system of $N(L)$ poles. The response to these perturbations gives us the rest of the stability spectrum; the combinations of these two steps rationalizes all the qualitative features found by traditional stability analysis.

In Sec. II we present a brief review of the stationary solutions of front propagation in channel geometries. In Sec. III we present the results of traditional linear stability analysis and show the eigenvalues and eigenfunctions that we want to interpret by using the pole decomposition. Section IV presents the analysis in terms of complex singularities, in two steps as discussed above. A summary and discussion is presented in Sec. V.

II. FLAME PROPAGATION IN CHANNEL GEOMETRY

We consider a two-dimensional channel of transverse width L and of infinite extent in the longitudinal direction. A

graph of a flame front propagating in this channel is defined as $h(x,t)$ with $0 < x < L$. A model that pertains to the propagation of this flame front was proposed in [5]. After appropriate rescalings it takes the form

$$\frac{\partial h(x,t)}{\partial t} = \frac{1}{2} \left[\frac{\partial h(x,t)}{\partial x} \right]^2 + \nu \frac{\partial^2 h(x,t)}{\partial x^2} + I\{h(x,t)\} + 1, \quad (1)$$

where ν is a parameter. The functional $I[h(x,t)]$ is the Hilbert transform that is conveniently defined in terms of the spatial Fourier transform

$$h(x,t) = \int_{-\infty}^{\infty} e^{ikx} \hat{h}(k,t) dk, \quad (2)$$

$$I[h(k,t)] = |k| \hat{h}(k,t). \quad (3)$$

This functional represents the Darrius-Landau instability and is the physical instability term. The first term in Eq. (1) has a geometric origin and it stems from a small tilt in the flame front with respect to the direction of propagation. The second term is the dissipative contribution that acts to reduce high wrinkling in the flame front. Rescaling further according to $x \rightarrow \theta = 2\pi x/L$, the new equation of motion for $h(\theta,t)$ is rewritten conveniently in terms of $u(\theta,t) \equiv \partial h(\theta,t)/\partial \theta$ [5–8]:

$$\frac{\partial u(\theta,t)}{\partial t} = \frac{u(\theta,t)}{L^2} \frac{\partial u(\theta,t)}{\partial \theta} + \frac{\nu}{L^2} \frac{\partial^2 u(\theta,t)}{\partial \theta^2} + \frac{1}{L} I\{u(\theta,t)\}. \quad (4)$$

It is very useful [4,9–11] to discuss the solutions of these equations of motion in terms of expansions in N poles whose position $z_j(t) \equiv x_j(t) + iy_j(t)$ in the complex plane is time dependent:

$$u(\theta,t) = \nu \sum_{j=1}^N \cot \left[\frac{\theta - z_j(t)}{2} \right] + \text{c.c.} \\ = \nu \sum_{j=1}^N \frac{2 \sin[\theta - x_j(t)]}{\cosh[y_j(t)] - \cos[\theta - x_j(t)]}, \quad (5)$$

Substituting Eq. (5) into Eq. (4), we derive the following ordinary differential equations for the positions of the poles:

$$-L^2 \frac{dx_j}{dt} = \nu \sum_{k=1, k \neq j}^N \sin(x_j - x_k) \times \{ [\cosh(y_j - y_k) - \cos(x_j - x_k)]^{-1} + [\cosh(y_j + y_k) - \cos(x_j - x_k)]^{-1} \}, \quad (6)$$

$$L^2 \frac{dy_j}{dt} = \nu \sum_{k=1, k \neq j}^N \left(\frac{\sinh(y_j - y_k)}{\cosh(y_j - y_k) - \cos(x_j - x_k)} + \frac{\sinh(y_j + y_k)}{\cosh(y_j + y_k) - \cos(x_j - x_k)} \right) + \nu \coth(y_j) - L. \quad (7)$$

In particular we can find the steady-state solution $u_s(\theta)$ by demanding $\dot{x}_j = \dot{y}_j = 0$ and stability. The solution is

$$u_s(\theta) = \nu \sum_{j=1}^N \frac{2 \sin[\theta - x_s]}{\cosh[y_j] - \cos[\theta - x_s]}, \quad (8)$$

where x_s is the real (common) position of the stationary poles and y_j their stationary imaginary position. We need to determine the actual positions y_j . This is done numerically by running the equations of motion for the poles starting from N poles in initial positions and waiting for relaxation. A complete analysis of this steady-state solution was presented in Ref. [4] and the main results are summarized as follows.

(i) There is only one stable stationary solution that is geometrically represented by a giant cusp (or, equivalently, one finger) and analytically by $N(L)$ poles that are aligned on one line parallel to the imaginary axis. The existence of this solution is made clearer with the following remarks.

(ii) There exists an attraction between the poles along the real line. This is obvious from Eq. (6), in which the sign of dx_j/dt is always determined by $\sin(x_j - x_k)$. The resulting dynamics merges all the x positions of poles whose y position remains finite.

(iii) The y positions are distinct and the poles are aligned above each other in positions $y_{j-1} < y_j < y_{j+1}$ with the maximum being $y_{N(L)}$. This can be understood from Eq. (7), in which the interaction is seen to be repulsive at short ranges, but changes sign at longer ranges.

(iv) If one adds an additional pole to such a solution, this pole (or another) will be pushed to infinity along the imaginary axis. If the system has less than $N(L)$ poles it is unstable to the addition of poles and any noise will drive the system towards this unique state. The number $N(L)$ is

$$N(L) = \left\lceil \frac{1}{2} \left(\frac{L}{\nu} + 1 \right) \right\rceil, \quad (9)$$

where the term in square brackets is the integer part. To see this consider a system with N poles and such that all the values of y_j satisfy the condition $0 < y_j < y_{max}$. Add now one additional pole whose coordinates are $z_a \equiv (x_a, y_a)$ with $y_a \gg y_{max}$. From the equation of motion for y_a [Eq. (7)] we see that the terms in the sum are all of the order of unity as is also the $\cot(y_a)$ term. Thus the equation of motion of y_a is approximately

$$\frac{dy_a}{dt} \approx \nu \frac{2N+1}{L^2} - \frac{1}{L}. \quad (10)$$

The fate of this pole depends on the number of other poles. If N is too large the pole will run to infinity, whereas if N is small the pole will be attracted towards the real axis. The condition for moving away to infinity is that $N > N(L)$, where $N(L)$ is given by Eq. (9). On the other hand, the y coordinate of the poles cannot hit zero. Zero is a repulsive line and poles are pushed away from zero with infinite velocity. To see this consider a pole whose y_j approaches zero. For any finite L the term $\coth(y_j)$ grows unboundedly, whereas all the other terms in Eq. (7) remain bounded.

(v) The height of the cusp is proportional to L . The distribution of positions of the poles along the line of constant x was worked out in [4].

We will refer to the solution with all these properties as the Thual-Frisch-Henon (TFH) cusp solution.

III. LINEAR STABILITY ANALYSIS IN CHANNEL GEOMETRY

The standard technique to study the linear stability of the steady solution is to perturb it by a small perturbation $\phi(\theta, t)$: $u(\theta, t) = u_s(\theta) + \phi(\theta, t)$. Linearizing the dynamics for small ϕ results in the equation of motion

$$\frac{\partial \phi(\theta, t)}{\partial t} = \frac{1}{L^2} \{ \partial_\theta [u_s(\theta) \phi(\theta, t)] + \nu \partial_\theta^2 \phi(\theta, t) \} + \frac{1}{L} I(\phi(\theta, t)), \quad (11)$$

where the linear operator contains $u_s(\theta)$ as a coefficient. Accordingly, simple Fourier modes do not diagonalize it. Nevertheless, we proceed to decompose $\phi(x)$ in Fourier modes according to

$$\phi(\theta, t) = \sum_{k=-\infty}^{\infty} \hat{\phi}_k(t) e^{ik\theta}, \quad (12)$$

$$u_s(\theta) = -2\nu i \sum_{k=-\infty}^{\infty} \sum_{j=1}^N \text{sgn}(k) e^{-|k|y_j} e^{ik\theta}. \quad (13)$$

Equation (13) follows from Eq. (8) by expanding in a series of $\sin k\theta$. In these sums the discrete k values run over all the integers. Substituting in Eq. (11) we get

$$\frac{d\hat{\phi}_k(t)}{dt} = \sum_n a_{kn} \hat{\phi}_n(t), \quad (14)$$

where a_{kn} are entries of an infinite matrix

$$a_{kk} = \frac{|k|}{L} - \frac{\nu}{L^2} k^2, \quad (15)$$

$$a_{kn} = \frac{k}{L^2} \text{sgn}(k-n) \left(2\nu \sum_{j=1}^N e^{-|k-n|y_j} \right), \quad k \neq n. \quad (16)$$

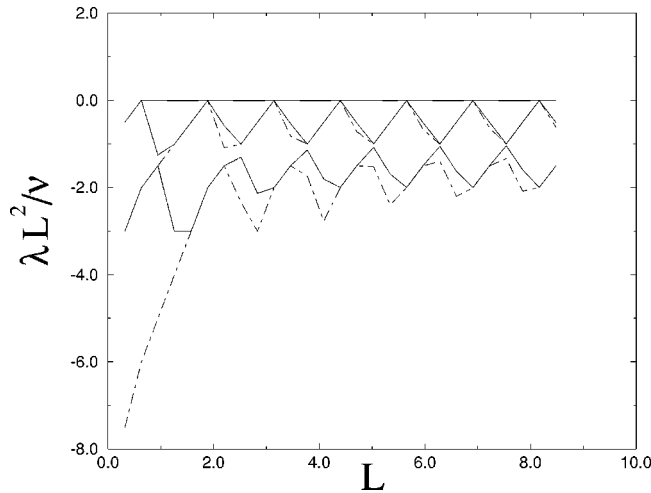


FIG. 1. Plot of the first five eigenvalues obtained by diagonalizing the matrix obtained by traditional stability analysis, against the system size. The eigenvalues are normalized by L^2/ν . The largest eigenvalue is zero, which is a Goldstone mode. All the other eigenvalues are negative except for the second and third, which touch zero periodically. The second and fourth eigenvalues are represented by a solid line and the third and fifth eigenvalues are represented by a dot-dashed line.

To solve for the eigenvalues of this matrix we need to truncate it at some cutoff k vector k^* . The scale k^* can be chosen on the basis of Eq. (15), from which we see that the largest value of k for which $a_{kk} \geq 0$ is a scale that we denote as k_{max} , which is the integer part of L/ν . We must choose $k^* > k_{max}$ and test the choice by the convergence of the eigenvalues. The chosen value of k^* in our numerics was $4k_{max}$. One should notice that this cutoff limits the number of eigenvalues, which should be infinite. However, the lower eigenvalues will be well represented. The results for the low-order eigenvalues of the matrix a_{kn} that were obtained from the converged numerical calculation are presented in Fig. 1.

The eigenvalues are multiplied by L^2/ν and are plotted as a function of L . We order the eigenvalues in decreasing order and denote them as $\lambda_0 \geq \lambda_1 \geq \lambda_2 \dots$. The figure offers a number of qualitative observations .

(i) There exists an obvious Goldstone or translational mode $u'_s(\theta)$ with eigenvalue $\lambda_0 = 0$. This eigenmode stems from the Galilean invariance of the equation of motion.

(ii) The eigenvalues oscillate periodically between values that are L independent in this presentation (in which we multiply by L^2). In other words, up to the oscillatory behavior the eigenvalues depend on L like L^{-2} .

(iii) The eigenvalues λ_1 and λ_2 hit zero periodically. The functional dependence in this presentation appears almost piecewise linear.

(iv) The higher eigenvalues are more negative. They exhibit similar qualitative behavior, but without reaching zero. We note that the solution becomes marginally stable for every value of L for which the eigenvalues λ_1 and λ_2 hit zero. The L^{-2} dependence of the spectrum indicates that the solution becomes more and more sensitive to noise as L increases [12].

In addition to the eigenvalues, the truncated matrix also yields eigenvectors that we denote as $A^{(\ell)}$. Each such vector

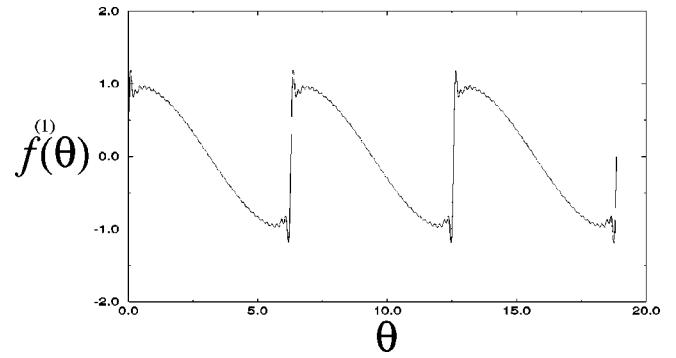


FIG. 2. First odd eigenfunction obtained from traditional stability analysis.

has k^* entries and we can compute the eigenfunctions $f^{(\ell)}(\theta)$ of the linear operator (11), using Eq. (12), as

$$f^{(\ell)}(\theta) \equiv \sum_{-k^*}^{k^*} e^{ik\theta} A_k^{(\ell)}. \quad (17)$$

Equation (11) does not mix even with odd solutions in θ , as can be checked by inspection. Consequently the available solutions have even or odd parity, expandable in either cos or sin functions. The first two nontrivial eigenfunctions $f^{(1)}(\theta)$ and $f^{(2)}(\theta)$ are shown in Figs. 2 and 3. It is evident that the function in Fig. 2 is odd around zero, whereas in Fig. 3 it is even. Similarly, we can numerically generate any other eigenfunction of the linear operator, but we understand neither the physical significance of these eigenfunction nor the L dependence of their associated eigenvalues shown in Fig. 1. In the next section we will demonstrate how the dynamical system approach in terms of singularities in the complex plane provides us with considerable intuition about these issues.

IV. LINEAR STABILITY IN TERMS OF COMPLEX SINGULARITIES

Since the partial differential equation is continuous there is an infinite number of modes. To understand this in terms of pole dynamics we consider the problem in two steps. First, we consider the $2N(L)$ modes associated with the dynamics of the $N(L)$ poles of the giant cusp. In the second step we explain that all the additional modes result from the

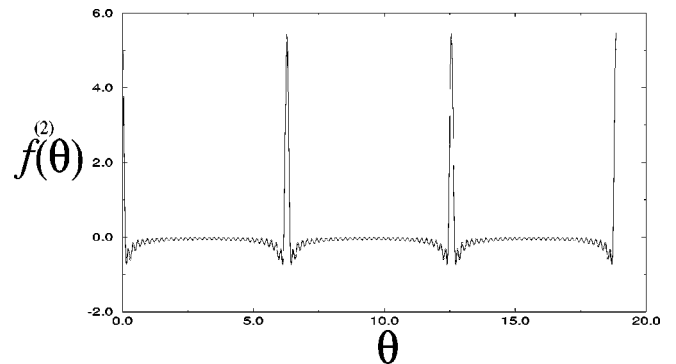


FIG. 3. First even eigenfunction obtained from traditional stability analysis.

introduction of additional poles, including the reaction of the $N(L)$ poles of the giant cusp to the new poles. After these two steps we will be able to identify all the linear modes that were found by diagonalizing the stability matrix in the preceding section.

A. Modes associated with the giant cusp

In the steady solution all the poles occupy stable equilibrium positions. The forces operating on any given pole cancel exactly and we can write matrix equations for small perturbations in the pole positions δy_i and δx_i .

Following [4], we rewrite the equations of motion (7) using the Lyapunov function U :

$$L\dot{y}_i = \frac{\partial U}{\partial y_i}, \quad (18)$$

where $i = 1, \dots, N$ and

$$U = \frac{\nu}{L} \left[\sum_i \ln \sinh y_i + 2 \sum_{i < k} \left(\ln \sinh \frac{y_k - y_i}{2} + \ln \sinh \frac{y_k + y_i}{2} \right) \right] - \sum_i y_i. \quad (19)$$

The linearized equations of motion for δy_i are

$$L\delta\dot{y}_i = \sum_k \frac{\partial^2 U}{\partial y_i \partial y_k} \delta y_k. \quad (20)$$

The matrix $\partial^2 U / \partial y_i \partial y_k$ is real and symmetric of rank N . We thus expect to find N real eigenvalues and N orthogonal eigenvectors.

For the deviations δx_i in the x positions we find the linearized equations of motion

$$L\delta\dot{x}_j = -\frac{\nu}{L} \delta x_j \sum_{k=1, k \neq j}^N \left(\frac{1}{\cosh(y_j - y_k) - 1} + \frac{1}{\cosh(y_j + y_k) - 1} \right) + \frac{\nu}{L} \sum_{k=1, k \neq j}^N \delta x_k \left(\frac{1}{\cosh(y_j - y_k) - 1} + \frac{1}{\cosh(y_j + y_k) - 1} \right) \quad (21)$$

or in shorthand

$$L \frac{d\delta x_i}{dt} = V_{ik} \delta x_k. \quad (22)$$

The matrix V is also real and symmetric. Thus V and $\partial^2 U / \partial y_i \partial y_k$ together supply $2N(L)$ real eigenvalues and $2N(L)$ orthogonal eigenvectors. The explicit form of the matrices V and $\partial^2 U / \partial y_i \partial y_k$ is as follows: For $i \neq k$

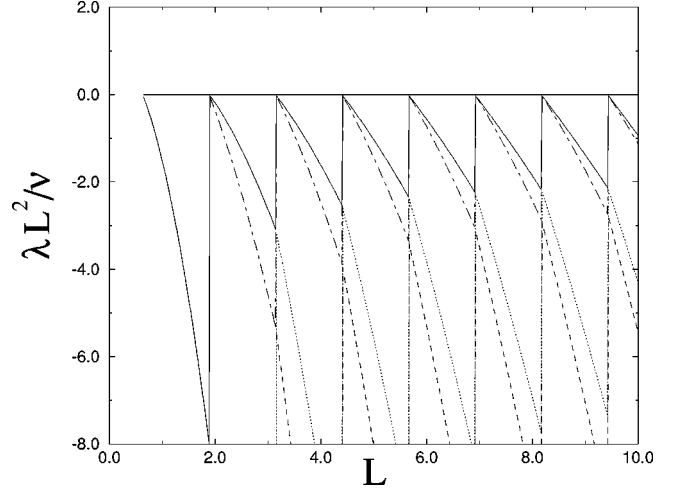


FIG. 4. Eigenvalues associated with perturbing the positions of the poles that consist in the giant cusp. The largest eigenvalue is zero. The second, third, fourth, and fifth eigenvalues are represented by a solid line, dot-dashed line, dotted line, and dashed line, respectively.

$$\frac{\partial^2 U}{\partial y_i \partial y_k} = \frac{\nu}{L} \left(\frac{1/2}{\sinh^2\left(\frac{y_k - y_i}{2}\right)} - \frac{1/2}{\sinh^2\left(\frac{y_k + y_i}{2}\right)} \right), \quad (23)$$

$$V_{ik} = \frac{\nu}{L} \left(\frac{1}{\cosh(y_i - y_k) - 1} + \frac{1}{\cosh(y_i + y_k) - 1} \right) \quad (24)$$

and for $i = k$

$$\frac{\partial^2 U}{\partial y_i^2} = -\frac{\nu}{L} \left[\sum_{k \neq i}^N \left(\frac{1}{2 \sinh^2\left(\frac{y_k - y_i}{2}\right)} + \frac{1}{2 \sinh^2\left(\frac{y_k + y_i}{2}\right)} \right) + \frac{1}{\sinh^2(y_i)} \right], \quad (25)$$

$$V_{ii} = \sum_{k \neq i}^N \left[-\frac{\nu}{L} \left(\frac{1}{\cosh(y_i - y_k) - 1} + \frac{1}{\cosh(y_i + y_k) - 1} \right) \right]. \quad (26)$$

Using the known steady-state solutions y_i at any given L we can diagonalize the $N(L) \times N(L)$ matrices numerically. In Fig. 4 we present the eigenvalues of the lowest-order modes obtained from this procedure. The least negative eigenvalues touch zero periodically. This eigenvalue can be fully identified with the motion of the highest pole $y_{N(L)}$ in the giant cusp. At isolated values of L the position of this pole tends to infinity and then the row and the column in our matrices that contain $y_{N(L)}$ vanish identically, leading to a zero eigenvalue. The rest of the upper eigenvalues match perfectly with half of the observed eigenvalues in Fig. 1. In other words, the eigenvalues observed here agree perfectly with the ones plotted in this Fig. 1 until the discontinuous increase from their minimal points. The ‘‘second half’’ of the oscillation in the eigenvalues as a function of L is not contained in this spectrum of the $N(L)$ poles of the giant cusp. To understand the

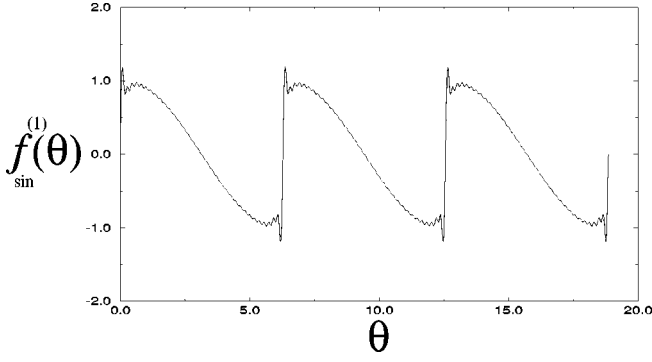


FIG. 5. First odd eigenfunction associated with perturbing the positions of the poles in the giant cusp.

rest of the spectrum we need to consider a perturbation of the giant cusp by additional poles.

The eigenfunctions can be found using the knowledge of the eigenvectors of these matrices. Let us denote the eigenvectors of $\partial^2 U / \partial y_i \partial y_k$ and V as $\mathbf{a}^{(\ell)}$ and $\mathbf{b}^{(\ell)}$, respectively. The perturbed solution is explicitly given as (for $x_s = 0$)

$$u_s(\theta) + \delta u = 2\nu \sum_{i=1}^N \frac{\sin(\theta - \delta x_i)}{\cosh(y_i + \delta y_i) - \cos(\theta - \delta x_i)}, \quad (27)$$

where δu is

$$\begin{aligned} \delta u = & -4\nu \sum_{i=1}^N \sum_{k=1}^{\infty} \delta y_i k e^{-ky_i} \sin k\theta \\ & -4\nu \sum_{i=1}^N \sum_{k=1}^{\infty} \delta x_i k e^{-ky_i} \cos k\theta. \end{aligned} \quad (28)$$

So knowing the eigenvectors $\mathbf{a}^{(\ell)}$ and $\mathbf{b}^{(\ell)}$, we can estimate the eigenvectors $f^{(\ell)}(\theta)$ of Eq. (17):

$$f_{\sin}^{(\ell)}(\theta) = -4\nu \sum_{i=1}^N \sum_{k=1}^{\infty} a_i^{(\ell)} k e^{-ky_i} \sin k\theta, \quad j = 1, \dots, N \quad (29)$$

or

$$f_{\cos}^{(\ell)}(\theta) = -4\nu \sum_{i=1}^N \sum_{k=1}^{\infty} b_i^{(\ell)} k e^{-ky_i} \cos k\theta, \quad j = 1, \dots, N \quad (30)$$

where we display separately the sin expansion and the cos expansion. For the case $\ell = 1$, the eigenvalue is zero and a uniform translation of the poles in any amount δx_i results in a Goldstone mode. This is characterized by an eigenvector $b_i^{(1)} = 1$ for all i . The eigenvectors $f^{(\ell)}$ (Figs. 5 and 6) computed this way are identical to numerical precision with those shown in Figs. 2 and 3 and observe the agreement.

B. Modes related to additional poles

In this subsection we identify the rest of the modes that were not found in the preceding subsection. To this aim we study the response of the TFH solution to the introduction of additional poles. We choose to add M new poles, all positioned at the same imaginary coordinate $y_p \ll y_{max}$, distrib-

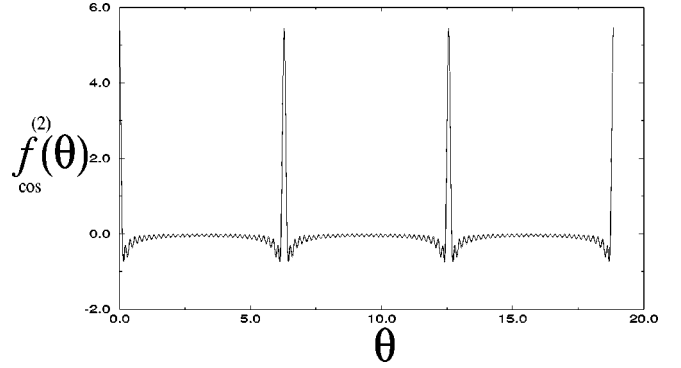


FIG. 6. First even eigenfunction associated with perturbing the positions of the poles in the giant cusp.

uted at equidistant real positions $\{x_j = x_0 + (2\pi/M)j\}_{j=1}^M$. For $x_0 = 0$ we use Eq. (5) and the Fourier expansion to obtain a perturbation of the form

$$\delta u(\theta, t) \approx 4\nu M e^{-My_p(t)} \sin M\theta. \quad (31)$$

For $x_0 = -\pi/2M$ we get

$$\delta u(\theta, t) \approx 4\nu M e^{-My_p(t)} \cos M\theta. \quad (32)$$

In both cases the equations for the dynamics of y_p follow from Eqs. (6) and (7):

$$\frac{dy_p}{dt} \approx 2\frac{\nu}{L^2} \alpha(M), \quad (33)$$

where $\alpha(M)$ is given as

$$\alpha(M) = \left[\frac{1}{2} \left(\frac{L}{\nu} + 1 \right) \right] - \frac{1}{2} \left(\frac{L}{\nu} - M \right). \quad (34)$$

Since Eq. (33) is linear, we can solve it and substitute in Eqs. (31) and (32). Seeking a form $\delta u(\theta, t) \sim \exp[-\lambda(M)t]$, we find that the eigenvalue $\lambda(M)$ is

$$\lambda(M) = 2M \frac{\nu}{L^2} \alpha(M). \quad (35)$$

These eigenvalues are plotted in Fig. 7.

At this point we consider the dynamics of the poles in the giant cusp under the influence of the additional M poles. From Eqs. (20), (22), (6), and (7) we obtain, after some obvious algebra,

$$L \delta \dot{y}_i = \sum_j \frac{\partial^2 U}{\partial y_i \partial y_j} \delta y_j - 4\frac{\nu}{L} M e^{-My_p(t)} \sinh(My_i) \quad (36)$$

or

$$L \delta \dot{x}_i = \sum_j V_{ij} \delta x_j - 4\frac{\nu}{L} M e^{-My_p(t)} \cosh(My_i). \quad (37)$$

It is convenient now to transform from the basis δy_i to the natural basis w_i , which is obtained using the linear transformation $\mathbf{w} = A^{-1} \delta \mathbf{y}$. Here the matrix A has columns that are the eigenvectors of $\partial^2 U / \partial y_i \partial y_j$ that were computed before.

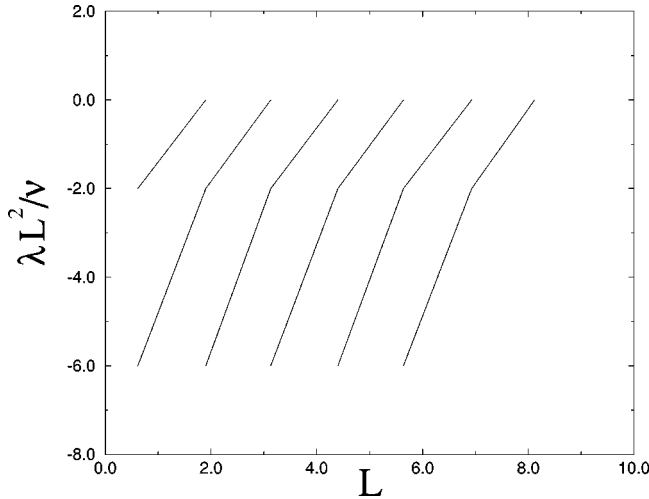


FIG. 7. Spectrum of eigenvalues associated with the reaction of the poles in the giant cusp to the addition of new poles.

Since the matrix was real symmetric, the matrix A is orthogonal and $A^{-1} = A^T$. Define $C = 4(\nu/L^2)M e^{-My_p(0)}$ and write

$$\dot{w}_i = -\lambda_i w_i - C e^{-\lambda(M)t} \xi_i, \quad (38)$$

where $-\lambda_i$ are the eigenvalues associated with the columns of A and

$$\xi_i = \sum_j A_{ji} \sinh My_j. \quad (39)$$

Since we are looking for an eigenvector, w_i is expected to decay exponentially with a rate $\lambda(M)$:

$$w_i(t) = w_i(0) e^{-\lambda(M)t}. \quad (40)$$

Substituting the desired solution in Eq. (38), we find a condition on the initial value of w_i :

$$w_i(0) = -\frac{C}{\lambda_i - \lambda(M)} \xi_i. \quad (41)$$

Transforming back to δy_i , we get

$$\begin{aligned} \delta y_i(0) &= \sum_k A_{ik} w_k(0) \\ &= -\sum_k A_{ik} \frac{C}{\lambda_k - \lambda(M)} \sum_l A_{lk} \sinh My_l \\ &= -C \sum_l \sinh My_l \sum_k \frac{A_{ik} A_{lk}}{\lambda_k - \lambda(M)}. \end{aligned} \quad (42)$$

We can get the eigenfunctions of the linear operator, as before, using Eqs. (28), (31), (32), and (42). We get

$$\begin{aligned} f_{\sin}^{(M)}(\theta) &= 4C\nu \sum_{i=1}^{N(L)} \sum_{k=1}^{\infty} \left(\sum_l \sinh My_l \sum_m \frac{A_{im} A_{lm}}{\lambda_m - \lambda(M)} \right) \\ &\quad \times k e^{-ky_i} \sin k\theta + L^2 C \sin M\theta. \end{aligned} \quad (43)$$

An identical calculation to the one started with Eq. (38) can be followed for the deviations δx_i . The final result reads

$$\begin{aligned} f_{\cos}^{(M)}(\theta) &= 4C\nu \sum_{i=1}^{N(L)} \sum_{k=1}^{\infty} \left(\sum_l \cosh My_l \sum_m \frac{\tilde{A}_{im} \tilde{A}_{lm}}{\tilde{\lambda}_m - \lambda(M)} \right) \\ &\quad \times k e^{-ky_i} \cos k\theta + L^2 C \cos M\theta, \end{aligned} \quad (44)$$

where \tilde{A} is the matrix whose columns are the eigenvectors of V and $-\tilde{\lambda}_i$ its eigenvalue.

We are now in position to explain the entire linear spectrum using the knowledge that we have gained. The spectrum consists of two separate types of contributions. The first type has $2N$ modes that belong to the dynamics of the unperturbed $N(L)$ poles in the giant cusp. The second part, which is most of the spectrum, is built from modes of the second type since M can go to infinity. This structure is seen in Figs. 4 and 7.

We can argue that the set of eigenfunctions obtained above is complete and exhaustive. To do this we show that any arbitrary periodic function of θ can be expanded in terms of these eigenfunctions. Start with the standard Fourier series in terms of sin and cos functions. At this point solve for $\sin k\theta$ and $\cos k\theta$ from Eqs. (43) and (44). Substitute the results in the Fourier sums. We now have an expansion in terms of the eigenmodes $f^{(M)}$ and in terms of the triple sums. The triple sums, however, can be expanded, using Eqs. (29) and (30), in terms of the eigenfunctions $f^{(\prime)}$. We can thus decompose any function in terms of the eigenfunctions $f^{(M)}$ and $f^{(\prime)}$.

V. CONCLUSIONS

We discussed the stability of flame fronts in channel geometry using the representation of the solutions in terms of singularities in the complex plane. In this language the stationary solution, which is a giant cusp in configuration space, is represented by $N(L)$ poles that are organized on a line parallel to the imaginary axis. We showed that the stability problem can be understood in terms of two types of perturbations. The first type is a perturbation in the positions of the poles that make up the giant cusp. The longitudinal motions of the poles give rise to odd modes, whereas the transverse motions give rise to even modes. The eigenvalues associated with these modes are eigenvalues of finite, real, and symmetric matrices; cf. Eqs. (23)–(26). The second type of perturbations is obtained by adding poles to the set of $N(L)$ poles representing the giant cusp. The reaction of the latter poles is again separated into odd and even functions, as can be seen from Eqs. (31) and (32). Together the two types of perturbations rationalize and explain all the features of the eigenvalues and eigenfunctions obtained from the standard linear stability analysis.

ACKNOWLEDGMENT

This work has been supported in part by the Israel Science Foundation administered by the Israel Academy of Sciences and Humanities.

- [1] P. Pelce, *Dynamics of Curved Fronts* (Academic, Boston, 1988).
- [2] A.-L. Barbási and H. E. Stanley, *Fractal Concepts in Surface Growth* (Cambridge University Press, Cambridge, 1995).
- [3] T. Viscek, *Fractal Growth Phenomena* (World Scientific, Singapore, 1992).
- [4] O. Thual, U. Frisch, and M. Henon, *J. Phys. (France)* **46**, 1485 (1985).
- [5] G.I. Sivashinsky, *Acta Astron.* **4**, 1177 (1977).
- [6] S. Gutman and G. I. Sivashinsky, *Physica D* **43**, 129 (1990).
- [7] O. Kupervasser, Z. Olami, and I. Procaccia, *Phys. Rev. Lett.* **76**, 146 (1996).
- [8] Z. Olami, B. Galanti, O. Kupervasser, and I. Procaccia, *Phys. Rev. E* **55**, 2649 (1997).
- [9] Y. C. Lee and H. H. Chen, *Phys. Scr.* **2**, 41 (1982).
- [10] G. Joulin, *J. Phys. (France)* **50**, 1069 (1989).
- [11] G. Joulin, *Zh. Eksp. Teor. Fiz.* **100**, 428 (1990).
- [12] B. Galanti, O. Kupervasser, Z. Olami, and I. Procaccia, *Phys. Rev. Lett.* **80**, 2477 (1998).